The performance of nitrate-reducing Fe(II) oxidation processes under variable initial Fe/N ratios: The fate of nitrogen and iron species

The performance of nitrate-reducing Fe(II) oxidation processes under variable initial Fe/N ratios: The fate of nitrogen and iron species

Journal:	*Frontiers of Environmental Science & Engineering*
Manuscript ID	FESE-2020-0225.R2
Manuscript Type:	Original Article
Date Submitted by the Author:	n/a
Complete List of Authors:	Cheng, Boyi; Huazhong Agricultural University Wang, Yi; Huazhong Agricultural University Hua, Yumei; Huazhong Agricultural University, Heal, Kate V.; University of Edinburgh, School of GeoSciences
Keywords:	Denitrification, N2O emission, Fe(II) oxidation, Fe/N ratio, Fe(III) (hydr)oxide minerals
Speciality:	Wastewater < WATER STUDIES, Lakes/streams/estuaries < WATER STUDIES, Environmental microbiology < BIOLOGICAL PROCESSES

Title: The performance of nitrate-reducing Fe(II) oxidation processes under variable initial Fe/N ratios: The fate of nitrogen and iron species

Running title: Response of nitrate-reducing Fe(II) oxidation processes to initial Fe/N ratio

Boyi Cheng[1], Yi Wang[1], Yumei Hua[1]*, Kate V. Heal[2]

1 College of Resources and Environment, Huazhong Agricultural University, Wuhan 430070, China

2 School of GeoSciences, University of Edinburgh, Edinburgh EH9 3FF, UK

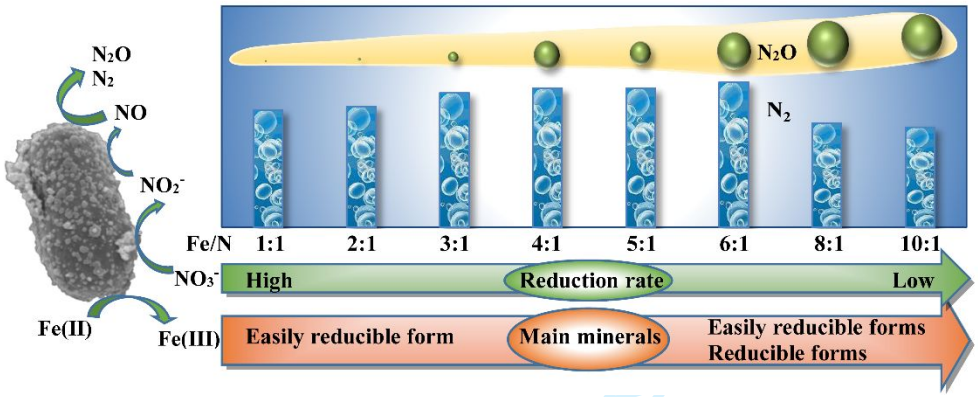

Highlights:

- Bacterially-mediated coupled N and Fe processes examined in incubation experiments
- NO_3^- reduction was considerably inhibited as initial Fe/N ratio increased
- The maximum production of N_2 occurred at an initial Fe/N molar ratio of 6
- Fe minerals produced at Fe/N ratios of 1-2 were mainly easily reducible oxides

Abstract: The Fe/N ratio is an important control on nitrate-reducing Fe(II) oxidation processes that occur both in the aquatic environment and in wastewater treatment systems. The response of nitrate reduction, Fe oxidation, and mineral production to different initial Fe/N molar ratios in the presence of *Paracoccus denitrificans* was investigated in 132 h incubation experiments. A decrease in the

nitrate reduction rate at 12 h occurred as the Fe/N ratio increased. Accumulated nitrite concentration at Fe/N ratios of 2-10 peaked at 12-84 h, and then decreased continuously to less than 0.1 mmol/L at the end of incubation. N_2O emission was promoted by high Fe/N ratios. Maximum production of N_2 occurred at a Fe/N ratio of 6, in parallel with the highest mole proportion of N_2 resulting from the reduction of nitrate (81.2%). XRD analysis and sequential extraction demonstrated that the main Fe minerals obtained from Fe(II) oxidation were easily reducible oxides such as ferrihydrite (at Fe/N ratios of 1-2), and easily reducible oxides and reducible oxides (at Fe/N ratios of 3-10). The results suggest that Fe/N ratio potentially plays a critical role in regulating N_2, N_2O emissions and Fe mineral formation in nitrate-reducing Fe(II) oxidation processes.

Keywords: Denitrification; N_2O emission; Fe(II) oxidation; Fe/N ratio; Fe minerals

1. Introduction

An excess presence of NO_3^- is harmful for aquatic ecosystems and human health, and hence NO_3^- removal has been the focus of many research efforts in natural aquatic environments and wastewater treatment (Zorgani et al., 2016; Han et al., 2019; Zhang et al., 2019). Biological denitrification is the main process of NO_3^- removal, for which the traditional electron donor is organic carbon. Inorganic substrates such as sulfur and Fe compounds can also act as electron donors for NO_3^- reduction (Melton et al., 2014). Fe is an abundant element in the environment, and plays an important role in both Fe and N cycles through nitrate-reducing Fe(II) oxidation (NRFO) bacteria (Straub et al., 1996; Weber et al., 2006; Melton et al., 2014). The contribution of NRFO to anoxic Fe(II) oxidation and the subsequent behavior is of great importance as NRFO bacteria have been discovered in a variety of habitats globally (Weber et al., 2006; Zhang et al., 2015).

Autotrophic N removal technologies mediated by NRFO bacteria have the advantage of minimising secondary pollution risk and have shown promise, especially for wastewater with a low C/N ratio (Zhang et al., 2014). However, autotrophic cultures based only on NO_3^- and Fe(II) generally result in slow growth of NRFO bacteria, while mixotrophic cultures based on NO_3^-, Fe(II) and organic cosubstrate (e.g., acetate) result in fast growth (Chakraborty et al., 2011; Jamieson et al., 2018). Moreover, most NRFO bacteria are described as mixotrophic (Klueglein and Kappler, 2013), such as *Paracoccus denitrificans* which was demonstrated to oxidize 84% of Fe(II) with an initial concentration of 4.5 mmol/L and reduce 0.7 mmol/L nitrate simultaneously in a pure culture (Muehe et al., 2009). As sediment in freshwater ecosystems contains accumulated organic carbon, mixotrophic NRFO bacteria may be predominant and play a significant role in the microbially mediated transformation of Fe(II) to Fe(III) in aquatic anoxic environments. Here, NO_3^- acts as the preferred electron acceptor based on energy considerations, and reactions between Fe and N may predominate (Melton et al., 2014; Liu et al., 2019).

Denitrification is a four-step reductive process through which NO_3^- is sequentially transformed into NO_2^-, NO, N_2O, and finally N_2 (Sparacino-Watkins et al., 2014), with the different products posing different impacts on human health and the environment. NO_2^- can cause methemoglobinemia and respiratory infections in humans (Watsuntorn et al., 2019). N_2O has a long atmospheric residence time of 114 years, behaves as a potent “greenhouse” gas and is the most significant contributor to stratospheric ozone depletion, negatively affecting human health, sensitive aquatic organisms and ecosystems (Zhu-Barker et al., 2015; Vasilaki et al., 2018). In contrast, N_2 does not have significant negative impacts and is the most desirable product of NO_3^- reduction.

Hence, more detailed knowledge of the processes involved in N transformation could help to improve understanding of the NRFO process and inform management of denitrification to minimise its negative by-products.

The reduction of NO_3^- by mixotrophic NRFO bacteria is coupled with the oxidation of Fe(II), resulting in the formation of various Fe (hydr)oxide minerals (Miot et al., 2015; Jamieson et al., 2018). The Fe minerals formed include ferrihydrite, green rust, goethite, lepidocrocite and magnetite, depending on various growth conditions (Posth et al., 2014). For example, *Acidovorax* sp. Strain BoFeN1, a strain of NRFO bacteria, is able to form different types of Fe minerals (Miot et al., 2009b), e.g., green rust (Klueglein and Kappler, 2013), goethite (Larese-C asanova et al., 2010) and lepidocrocite (Liu et al., 2019), under different conditions. Fe minerals can precipitate on the surface of bacteria and decrease the metabolic efficiency of NO_3^- reduction (Miot et al., 2015; Chen et al., 2018). However, Fe minerals also provide a positive control on the cycling of contaminants such as phosphorus and metal/metalloids, through their adsorption on Fe minerals with a high specific surface area (Pownceby et al., 2019), thus influencing the transport and fate of these species in natural environments and wastewater treatment systems. Since the adsorption capacity of Fe minerals together with their environmental behavior are related to their mineralogy, it is important to identify the Fe minerals produced in the NRFO process.

According to theoretical equations, Fe/N molar ratios may affect the products of NO_3^- reduction during the NRFO process through the catalysis of some chemicals including Fe(III) (hydr)oxide minerals, green rust, pyrite, and Cu^{2+} (Straub et al., 1996; Ottley et al., 1997; Picardal, 2012), and subsequently the environmental impact of different denitrification products. Conversely,

Fe minerals with different effective behaviors for removing toxic metals (e.g., As and Cr) and phosphorus during Fe(II) oxidation may also be produced at different Fe/N ratios. The effect of Fe/N molar ratios (1-6) on NO_3^- removal efficiency has been reported (Zhang et al., 2014), but the denitrification products (i.e., NO_2^-, N_2O and N_2) and Fe minerals mediated by Fe/N molar ratio have not been clarified yet. Hence, using *Paracoccus denitrificans* the current research aims to investigate the performance of NRFO at different initial Fe/N molar ratios, during which the products in the headspace gas, aqueous phase and precipitates were investigated to explore the fate of N and Fe.

2. Materials and methods

2.1. Bacterial strain and medium

Paracoccus denitrificans (CCTCC AB2013117) was purchased from China Center for Type Culture Collection and first activated in a beef extract-peptone medium at 30 °C. The bacteria were cultured to the exponential phase using the spread plate method, reaching a concentration of 1.5×10^8 cell/mL. The cells were harvested by centrifugation (5,000 rpm, 30 min, 30 °C), washed twice with a PIPES buffer (10 mmol/L, pH 7.0), and then resuspended as an inoculum for the different experimental treatments.

The experimental medium solution, containing 0.3 g/L NH_4Cl, 0.5 g/L KH_2PO_4, 0.1 g/L $CaCl_2{\cdot}2H_2O$, and 0.5 g/L $MgSO_4{\cdot}7H_2O$, was autoclaved and cooled. Then $NaHCO_3$ solution, trace element mixture SL8, vitamins, and sodium acetate solution were filter-sterilized (0.22 μm), placed in a UV sterilization station (SW-CJ-2FD, China) and added (Ehrenreich and Widdle, 1994; Muehe et al., 2009), so that the initial sodium acetate concentration in the medium was 1 mmol/L. The

medium pH was adjusted to 7.0 with NaOH solution (~ 0.1 mol/L) in a UV sterilization station (SW-CJ-2FD, China).

2.2. Experimental procedure

Five mL of cell suspension were added to 118-mL serum bottles containing 93 mL of medium deoxygenated by O_2-free ultrapure Ar gas. Eight treatments were set up as follows. The parallel serum bottles were purged with O_2-free ultrapure Ar gas for at least 2 min (0.6 L/min flux) to replace the headspace air. The NO_3^- concentration in all bottles was 1 mmol/L from the addition of 1 mL $NaNO_3$ solution. One mL $FeSO_4 \cdot 7H_2O$ solution was added at concentrations of 100, 200, 300, 400, 500, 600, 800, and 1000 mmol/L in each bottle separately before the end of the Ar gas purging, resulting in initial Fe/N molar ratios of 1, 2, 3, 4, 5, 6, 8, and 10. The Fe(II) stock solutions were prepared by adding $FeSO_4 \cdot 7H_2O$ to anoxic (100% Ar headspace) deoxygenated water and then sealing the bottle with a butyl stopper under an anoxic atmosphere (100% Ar headspace). The time at which the incubation bottles were quickly sealed with butyl rubber septa and an aluminium crimp was recorded as 0 h. Two needles fitted with a three-way valve were inserted into each butyl rubber septa for gas and solution sampling, respectively. At 0, 12, 36, 60, 84, 108, and 132 h, serum bottles for each set of treatments were removed for destructive sampling to determine the pH, as well as the NO_3^-, NO_2^-, Fe(II), Fe(III), and dissolved organic carbon (DOC) contents (Fig. 1). Precipitate samples were collected at the end of the experiment at 132 h via a filter syringe (0.22 μm). Then, the precipitates collected on 0.22 μm filter were washed twice with deoxygenated water and freeze-dried (-80 °C) (SCIENTZ-18N, China) before determination of different Fe fractions. All experiments were performed in triplicate and cultivated at 30 °C.

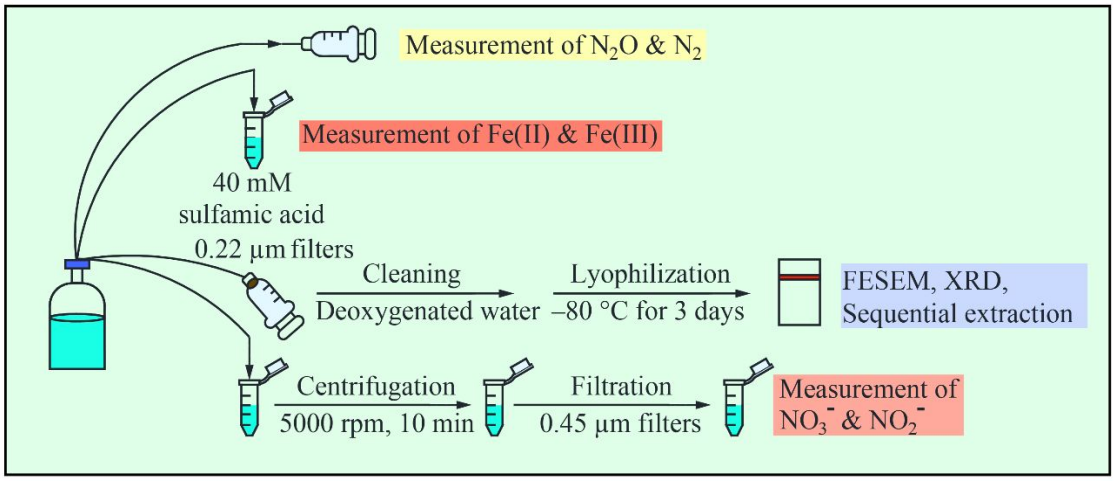

Fig. 1. Schematic representation of the sampling and pretreatment processes for gas, liquids, and precipitates from the experimental bottles.

2.3. Sample analysis and calculations

The ferrozine assay was used to determine the concentration of Fe(II) in the dissolved phase, after mixing sampled culture suspensions with 40 mmol/L sulfamic acid (pH~1.8) (Klueglein and Kappler, 2013). Total Fe content was determined by reducing an aliquot of the sample with hydroxylamine hydrochloride before addition of the ferrozine reagent (Stookey, 1970). Fe(III) content was calculated by subtracting the Fe(II) content from the total Fe content. A pH meter (Mettler Toledo, Switzerland) was used to determine the pH value. Other suspension samples were placed in an UV sterilization station to kill all cells (SW-CJ-2FD, China) and then fully exposed to O_2, to induce oxidation of Fe(II) (Chen et al., 2018). Subsequently, they were centrifuged (5,000 rpm, 10 min) to remove both the cells and the Fe oxides and then filtered through a 0.45 μm membrane before determination of NO_3^--N, NO_2^--N (APHA, 2012) and DOC concentrations using a total organic carbon analyzer (Vario TOC cube, Elementar, Germany).

Contents of N_2O and N_2 in headspace samples were determined by gas chromatography using

an Agilent 7890A (USA) equipped with an electron capture detector and an Agilent 7890B (USA), respectively.

The morphology of the precipitates was investigated using a field emission scanning electron microscope (FESEM, GeminiSEM 300, Germany) at 5 kV. The type of Fe minerals in the precipitates was identified with an X-ray diffractometer (Bruker, Germany) using Cu Kα filtered radiation. The precipitate samples were scanned between 5-80° 2θ using a step size of 0.02° and a scan speed of 1.0° 2θ min^{-1}. MDI Jade 6.5 was used to identify the mineral phases. A sequential extraction procedure (Fig. A1) was applied to the precipitates to fractionate Fe into the following forms: carbonate associated (Fe_{carb}), easily reducible oxides (Fe_{ox1}), reducible oxides (Fe_{ox2}), magnetite (Fe_{mag}), poorly reactive sheet silicate (Fe_{prs}), and unreactive silicate (Fe_U) (Poulton and Canfield, 2005; Ma et al., 2019). Fe concentration was determined using ferrozine method (Stookey, 1970) in aliquots of the solution resulting from each extraction step. Additionally, total Fe was extracted from the precipitate using 0.5 mol/L HCl (Wang et al., 2016) and measured with the ferrozine method (Stookey, 1970).

2.4. Statistical analysis

Duncan's multiple range tests were performed using SPSS 20.0 software to identify any significant differences between samples. Correlative analyses were performed using Pearson's correlation.

3. Results

3.1. Variation in NO_3^- and NO_2^- concentrations

Generally, the NO_3^- concentration in all treatments decreased with time (Fig. 2a). At 12 h, the NO_3^- concentration was very similar (0.41-0.44 mmol/L) for treatments with Fe/N ratios of 4-10,

but was only 0.08 mmol/L at Fe/N ratio of 1. NO_3^- reduction rates at 12 h in treatments with Fe/N ratio of 1 and 2 (76.8 and 60.9 μmol/L/h respectively) were higher than in treatments with Fe/N ratios of 4–10 (46.5–53.4 μmol/L/h). At the end of the incubation, the reduction in the initial NO_3^- concentration was ~95%, except for in the treatments with Fe/N ratios of 8 and 10, which had significantly lower NO_3^- consumption than other treatments (Table A1).

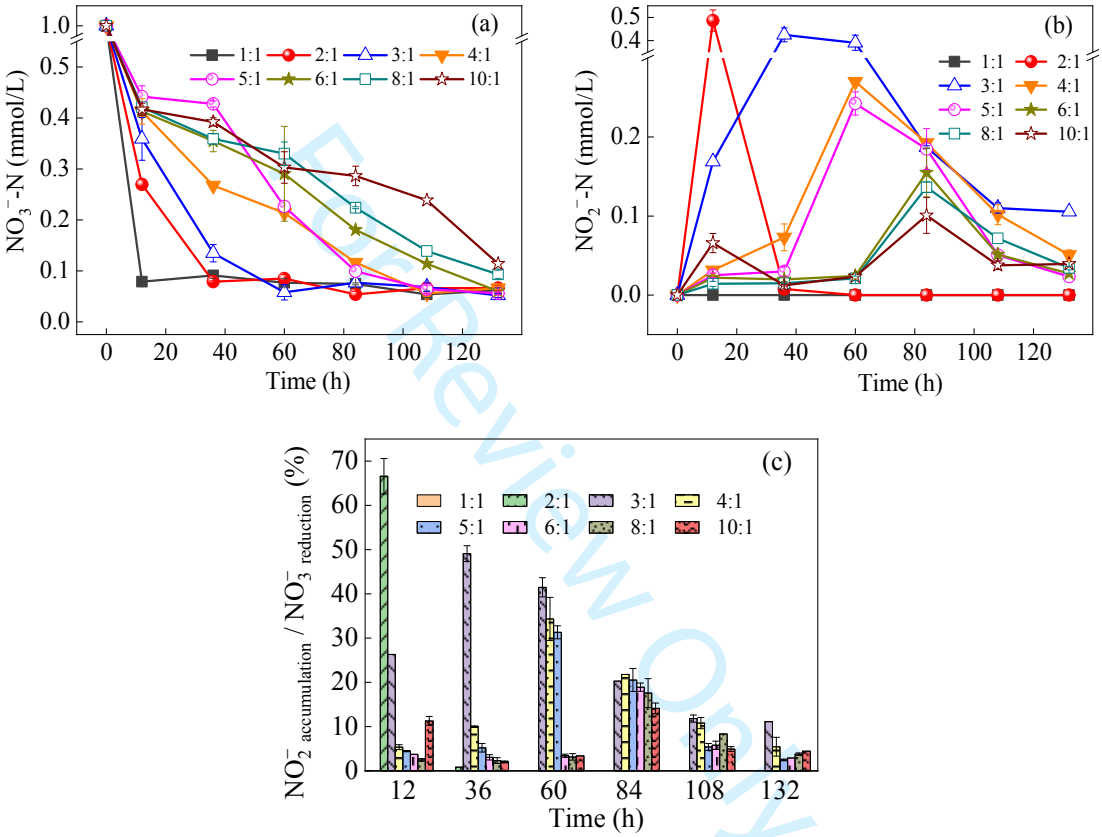

Fig. 2. NO_3^- concentration (a), NO_2^- concentration (b), and NO_2^- accumulation expressed as a % of NO_3^- reduction (c) during the incubation. The NO_2^- concentration at a Fe/N ratio of 1 was zero throughout the incubation, and that at a Fe/N ratio of 2 fell to zero after 36 h. Values are means (n=3) and error bars in (a) and (b) represent the standard deviation.

The timing and magnitude of peak NO_2^- concentration, a common intermediate of denitrification, varied between treatments with different Fe/N ratios (Fig. 2b). The detection of no

NO_2^- in the Fe/N ratio 1 treatment was probably attributed to the fast reduction with a suitable pH of this treatment (Fig. A3) (Buchwald et al., 2016) and the lower inhibiting effect on cell growth by Fe mineral encrustation. NO_2^- accumulation was detected at Fe/N ratios of 2-10, first increasing and then decreasing, with peak magnitude decreasing and peak timing increasing as Fe/N ratio increased from 2 to 10. A similar pattern was evident in NO_2^- accumulation expressed as a % of NO_3^- reduction during the incubation (Fig. 3c). The peak percentage of NO_2^- to NO_3^- reduction was 66.6% for the Fe/N ratio 2 treatment at 12 h, much higher than that for other treatments, whilst the peak percentage for Fe/N ratios of 3-5 occurred during 12-60 h. The initial Fe/N ratio of 2 would favor NO_2^- production from a stoichiometric point of view (Ottley et al., 1997) as illustrated in Eq. 3:

$$2\ Fe^{2+} + NO_3^- + 3\ H_2O \rightarrow 2\ FeOOH + NO_2^- + 4\ H^+ \quad \text{(Eq. 3)}.$$

A large NO_2^- accumulation (equivalent to >30% of the reduced NO_3^-) was observed at Fe/N ratios of 2–5 within 60 h, but at 132 h NO_2^- concentrations in all Fe/N ratio treatments were below 0.11 mmol/L.

3.2. N_2O and N_2 emissions

The N_2O production in the headspace was below 0.006 μmol at Fe/N ratios of 1-3 throughout the incubation, while it generally showed an increasing tendency at Fe/N ratios of 4-10 (Fig. 3a). By comparison, the N_2O production at the Fe/N ratio of 10 at 12 h was 0.003 μmol, ~10 times higher than that for the Fe/N ratio of 1 at 12 h, and further increased to ~700 times higher at 132 h.

The N_2 production at all Fe/N ratios showed a substantial increase in the first 12 h (Fig. 3b), consistent with the drastic decrease in NO_3^- concentrations. The highest N_2 production was 82.2

μmol at 108 h for the Fe/N ratio of 6, and this ratio maintained the highest N_2 production throughout the incubation compared to the other Fe/N ratios, apart from at 84 h. At 84 h, 108 h and 132 h, the N_2 production in treatments with Fe/N ratios of 8–10 were lower compared to those in other treatments.

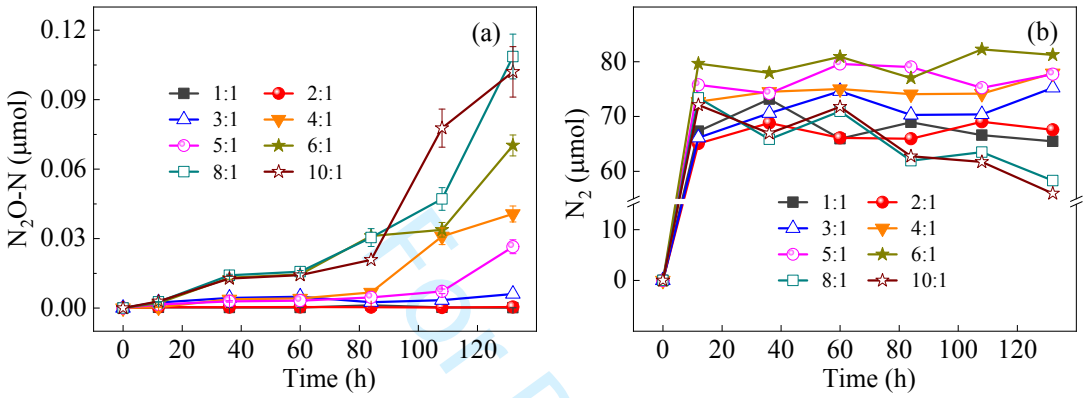

Fig. 3. N_2O production (a) and N_2 production (b) in the headspace at different Fe/N ratios during the incubation.

3.3. Fe(II) oxidation and precipitate characterization

A rapid oxidation of the aqueous Fe(II) concentration combined with an immediate increase of Fe(III) concentration was observed at 12 h in the incubation (Fig. 4a). In treatments with Fe/N ratios of 1–5, the Fe(II) oxidation rates followed the pattern of a pseudo-first-order reaction in the first 60 h. The corresponding reaction rate constants (k) were 0.015 h^{-1} (R^2 = 0.818), 0.023 h^{-1} (R^2 = 0.723), 0.032 h^{-1} (R^2 = 0.934), 0.032 h^{-1} (R^2 = 0.947) and 0.030 h^{-1} (R^2 = 0.909). A minor decrease in Fe(II) concentrations was observed in all treatments after 60 h. At 132 h, >82% of the initial Fe(II) had been oxidized at Fe/N ratios of 1–5, and a linear relationship was observed between N_2 emission (y) and Fe(II) concentrations in the medium (x) (Fig. A4). The decrease in Fe(II) concentrations during the incubation ranged from 0.83 mmol/L (at a Fe/N ratio of 1) to 6.10 mmol/L(at a Fe/N ratio of 10). The Fe(III) concentrations in solution peaked at 12 h, and were

lower than 0.26 mmol/L in all the treatments throughout the experiment (Fig. 4b). The % decrease in initial Fe(II) concentrations was higher at lower Fe/N ratios (Fig. 4c), and significant differences in Fe(II) consumption between Fe/N ratios of 1-4 and Fe/N ratios of 5-10 were observed at 132 h (Table A1).

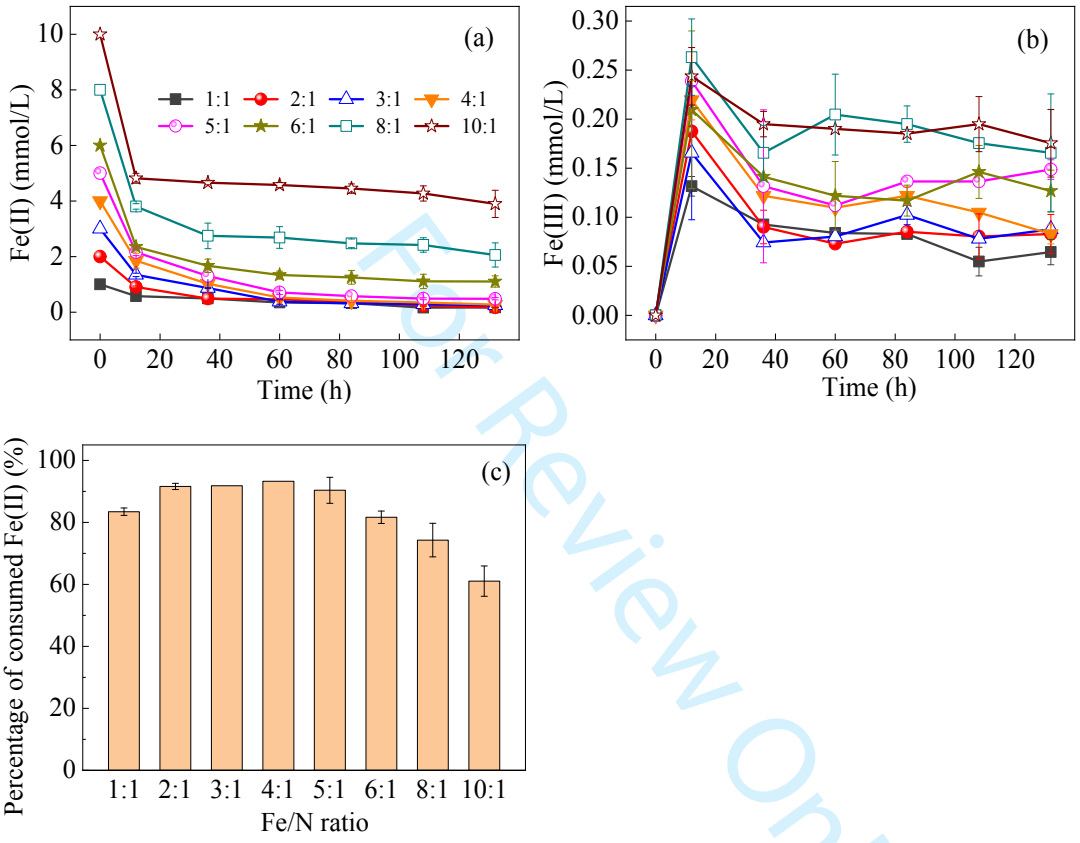

Fig. 4. Dissolved Fe(II) concentrations (a), dissolved Fe(III) concentrations (b) during the incubation, and consumption percentages of Fe(II) at 132 h (c). Values are means (n=3) and error bars in (a), (b) and (c) represent the standard deviation.

FESEM images showed that the precipitates covering cell surfaces at 60 h were similar among treatments with Fe/N ratios of 1–3 (Fig. 5a-c). Finer precipitates occurred on the cells at Fe/N ratios > 4 (Fig. 5d-f). Small holes were apparent on the surface of cells at a Fe/N ratio of 8 (Fig. 5g-h). Their formation may be attributed to the accumulation of Fe aggregates on the periplasm and the consequent destruction of the cell membrane. As a result, the holes would have become visible once

the accumulation of Fe aggregates reached a critical threshold and detached from the cell surface.

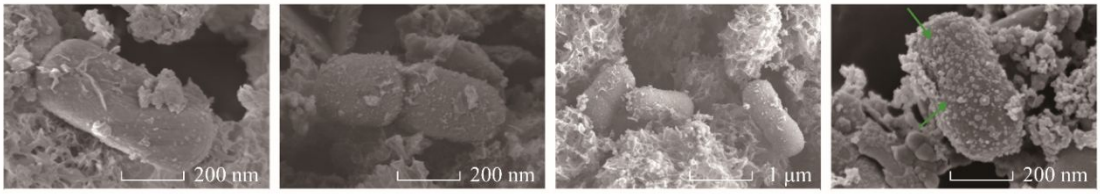

(a) Fe/N = 1:1 (b) Fe/N = 2:1 (c) Fe/N = 3:1 (d) Fe/N = 4:1

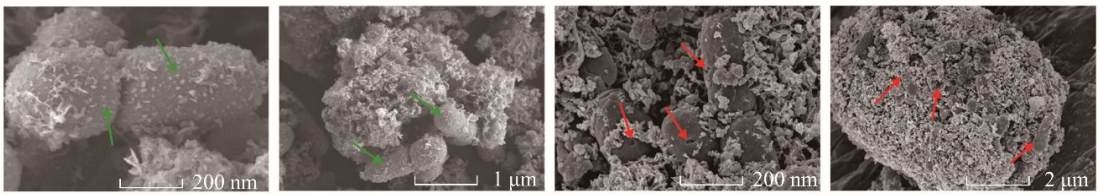

(e) Fe/N = 5:1 (f) Fe/N = 6:1 (g) Fe/N = 8:1 (h) Fe/N = 10:1

Fig. 5. FESEM images of precipitates from treatments with different Fe/N ratios at 60 h. Green arrows indicate precipitates, and red arrows indicate small holes on cell surfaces.

For the treatments at Fe/N ratio of 1 and 2, the most obvious peaks in the XRD analysis of the precipitates were at 132 h, rather than at 12 h and 60 h, whilst the pattern of peaks was similar in all time steps for treatments of Fe/N ratios 3-10 (Fig. 6). The XRD patterns showed that the dominant mineral phases in precipitates were goethite (α-FeOOH) and 2-line ferrihydrite ($Fe_5HO_8 \cdot 4H_2O$), with two characteristic peaks (2θ = 34°, 61°) (Das et al., 2011). A marginal fraction was represented by magnetite (Fe_3O_4), which had a characteristic peak at 35.62°. Some peaks of vivianite ($Fe_3(PO_4)_2) \cdot 8H_2O$) (Zhao et al., 2013) were identified in all treatments, consistent with the observation of the white precipitates formation after Fe(II) addition to the medium.

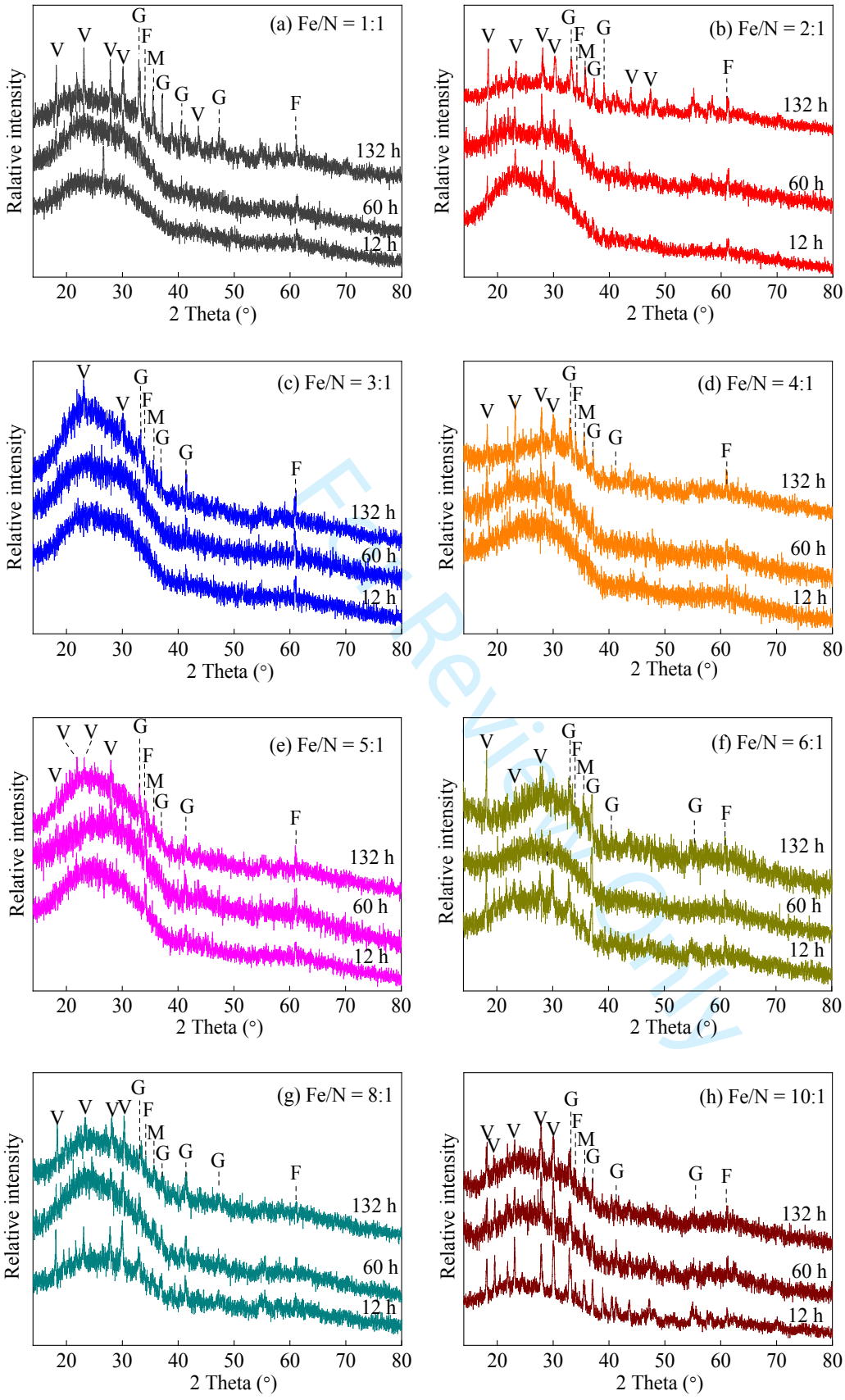

Fig. 6. X-ray diffraction patterns of the precipitates from different Fe/N ratio treatments at 12, 60 and 132 h. V

represents vivianite, G represents goethite, F represents ferrihydrite and M represents magnetite.

Total Fe concentrations in the precipitates ranged between 196 and 336 mg/g, and generally increased with the Fe/N ratio (Table A2). The Fe fractions Fe_{ox1} (easily reducible oxides) and Fe_{ox2} (reducible oxides) accounted for the majority of Fe in the precipitates at 132 h (Fig. 7), although the sum percentage of these two fractions generally decreased with increasing Fe/N ratio, from 91.8% at a Fe/N ratio of 1 to 65.5% at a Fe/N ratio of 10. The % of Fe occurring in the unreactive silicate form (Fe_U) generally increased with Fe/N ratio from 6.78% to 30.7% at Fe/N ratios of 1 and 10, respectively. Fe_{carb} accounted for the next largest proportion (0.9%–3.5%) in the precipitates at 132 h. The Fe_{mag} content was highest at a Fe/N ratio of 2 (0.39 mg/g) compared to other Fe/N ratios (0.07–0.22 mg/g), in accord with an obvious peak of magnetite at a Fe/N ratio of 2 in the XRD results (Fig. 6b), but accounted for a negligible fraction of Fe in the precipitates (<0.16%). Similarly, poorly reactive sheet silicate (Fe_{prs}) accounted for only 0.03-0.58% of the total Fe in precipitates after 132 h incubation.

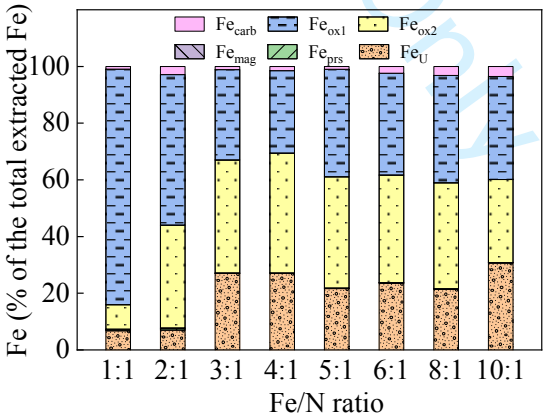

Fig. 7. Fe speciation of the precipitates from different Fe/N ratio treatments after 132 h incubation. For explanation of the different Fe fractions in the legend see text in Section 2.3.

4. Discussion

4.1. The fate of N

NRFO is expected to be an important pathway for N removal in Fe-rich habitats, yielding energy for carbon assimilation into biomass and microbial growth (Weber et al., 2006). The pathways of reduction of NO_3^- and its intermediate products in the current study may include: autotrophic biological reduction with Fe(II) as the electron donor, heterotrophic biological reduction with organic substrates as the electron donor, and abiotic reduction (i.e., chemodenitrification). In the current mixotrophic incubation, acetate and Fe(II) were both electron donors competing for NO_3^- as the acceptor. Acetate was consumed prior to Fe(II) in NRFO cultures of *Azospira siullum* strain PS under acceptor-limited conditions (Carlson et al., 2013). Although a rapid decrease in the dissolved Fe(II) concentrations occurred at 12 h for all treatments in the current study, it may be due to the production of vivianite (as evidenced by the XRD analysis results, Fig. 6) instead of consumption as an electron donor in NO_3^- reduction.

At 132 h, higher Fe(II) consumption accompanied by lower DOC consumption (Fig. A2; Table A1) occurred as Fe/N ratio increased, which could be attributed to the prevention of carbon assimilation by periplasmic Fe encrustation and relative inhibition of heterotrophic biological reduction (Miot et al., 2015) with increasing Fe/N ratio. These tendencies could also be attributed to an increasing role of chemodenitrification or autotrophic biological reduction at higher Fe/N ratios. The lower pH solution values at higher Fe/N ratios (Fig. A3) supported this interpretation as the process of N heterotrophic biological reduction produces alkalinity, in contrast to the production of acidity by chemodenitrification and autotrophic biological reduction (Straub et al., 1996). However, it was not possible in the current study to identify which of the autotrophic biological reduction or

chemodenitrification pathways dominated Fe(II) consumption. From a stoichiometric point of view, the oxidation of Fe(II) couldn't provide sufficient electrons for nitrate reduction to N_2 when the Fe/N ratio was less than 5. Organic carbon was consumed to supplement electrons and the consumed organic carbon decreased with the increasing Fe/N ratio (Table A1).

Decreasing NO_3^- reduction was observed as Fe/N ratio increased, suggesting that a high Fe/N ratio inhibited the utilization of NO_3^- by *Paracoccus denitrificans*. This finding is aligned with those from other studies so that possible mechanisms for the role of Fe minerals in the NRFO process can be proposed (Fig. 8). Similar experiments conducted in a mixotrophic medium reported that cells were heavily encrusted by Fe minerals at an initial Fe(II) concentration of 8 mmol/L, lost their motility and were unable to utilize acetate and NO_3^- as substrates for heterotrophic growth (Chakraborty et al., 2011). Furthermore, the coverage of Fe aggregates on the cell surface affected cell growth, and even caused the death of cells (Miot et al., 2015). The cell growth is closely related to enzyme activity. Membrane-bound and periplasmic NO_3^- reductase enzymes have been shown to be expressed in *Paracoccus denitrificans*, with the former playing a dominant role in NO_3^- reduction under anaerobic conditions and having an active site in the cytoplasm (Sears et al., 1997). As the insoluble Fe aggregates cannot diffuse into microbial cells, the encrustations of Fe minerals observed in the periplasm could not directly influence the active site of the membrane-bound NO_3^- reductase in the cytoplasm and subsequent denitrification (Sparacino-Watkins et al., 2014). However, the Fe minerals probably inhibited the NO_3^- scavenging ability of cells, and hence probably contributed to the decreased NO_3^- reduction rate (Fig. 8).

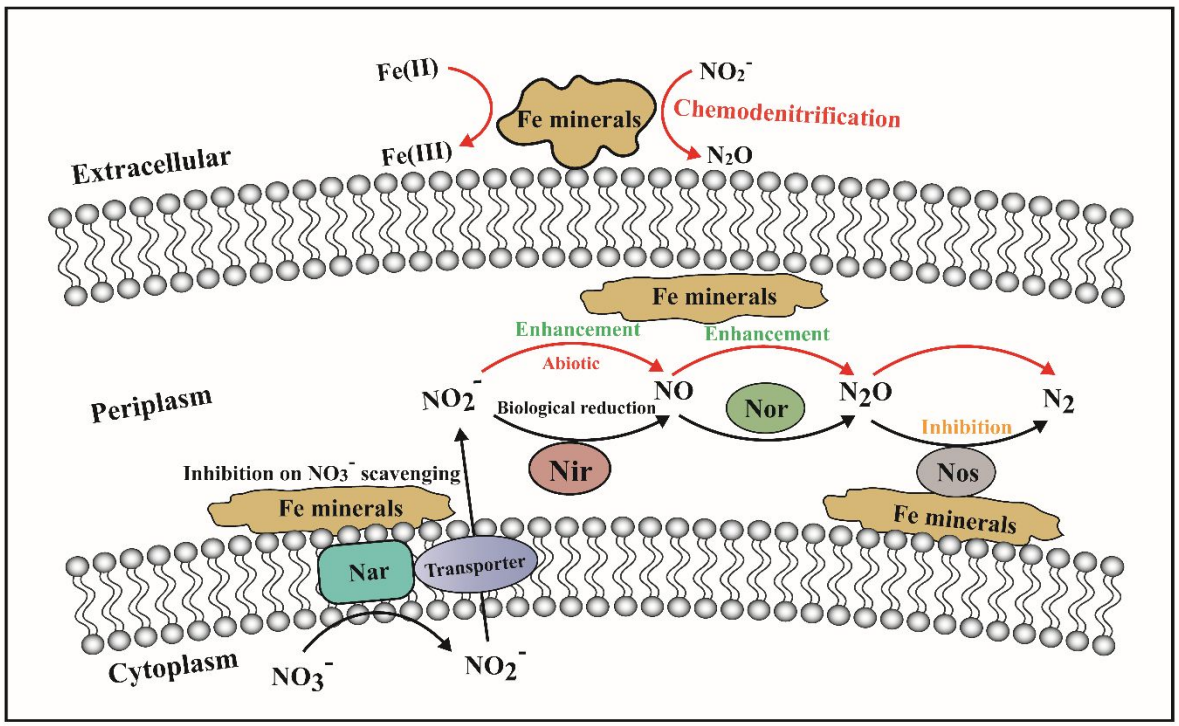

Fig. 8. Possible mechanisms for the role of Fe minerals in the NRFO process mediated by bacteria. Chemodenitrification is indicated by red arrows and biological reduction is indicated by black arrows. Nar, nitrate reductase; Nir, nitrite reductase; Nor, nitric oxide reductase; Nos, nitrous oxide reductase.

Differences in NO_2^- accumulation between the different treatments in the current study suggest that the rate of N reduction after the transformation of NO_3^- to NO_2^- was affected by the Fe/N ratio. Chakraborty et al. (2011) reported that NO_2^- accumulation occurred only when Fe(II) was present, indicating the inhibiting effect of concomitant Fe(II) oxidation on NO_2^- reduction during the NRFO process. NO_2^- reductase occurring in the periplasm (Sears et al., 1997) may become coated by Fe minerals, leading to a decrease in the NO_2^- reduction rate (Fig. 8) and the accumulation of NO_2^-. If only the negative effect of Fe minerals covering was considered, high NO_2^- accumulation should have been observed as Fe/N ratio increased. However, NO_2^- accumulation decreased as Fe/N ratio

increased from 2 to 10 (Fig. 2b), suggesting some other internal process accelerating NO_2^- reduction. Indeed, the rapid formation of Fe minerals during the NRFO process may provide a secondary and presumably faster pathway for NO_2^- reduction (Buchwald et al., 2016), in which Fe minerals can play a positive role in NO_2^- reduction through chemodenitrification (Eq. 4), since a strong chemical potential exists between Fe(II) and NO_2^- (Carlson et al., 2012; Klueglein and Kappler, 2013):

$$4\ Fe(II) + 2\ NO_2^- + 5\ H_2O \rightarrow 4\ FeO(OH) + N_2O + 6\ H^+ \quad \text{(Eq. 4)}$$

The Gibbs free energies of Eq. 4 are −147.6 kJ/mol e^-, indicating that the chemical reactions between Fe(II) and nitrite are thermodynamically feasible (Liu et al., 2019). Rates of Fe(II) oxidation and NO_2^- reduction for chemodenitrification were shown to increase simultaneously in the pH range 5.5-7.0 in a study involving pH effect and mineral formation on the interaction between NO_2^- and Fe(II) (Chen et al., 2020). In the chemodenitrification process, the reduction of NO_2^- by Fe(II) can be catalyzed by Fe minerals (Fig. 8), such as magnetite and goethite (Buchwald et al., 2016; Grabb et al., 2017). Hence, the Fe minerals produced at high Fe/N ratios can have a dual effect on the NO_2^- reduction process. Fe minerals (e.g., ferrihydrite, goethite and magnetite) on cell surfaces may act to accelerate chemodenitrification, while Fe minerals in the periplasm may inhibit NO_2^- reduction. From biogeochemical modeling of NRFO experiments, Jamieson et al. (2018) showed that chemodenitrification could be responsible for 40% of the overall dissolved Fe(II) oxidized by *Paracoccus denitrificans* in media with acetate, with the accompanying biotic NRFO accounting for the remaining oxidation. As more Fe minerals were produced at higher Fe/N ratios than lower ratios, in the current study chemodenitrification probably played a greater role in

NO_2^- reduction. In addition, the Fe minerals formed associated with the biologically-mediated component of NRFO (i.e. goethite, and magnetite) differ from those formed by chemodenitrification (only goethite) (Liu et al., 2019).

Processes involving N are closely associated with greenhouse gas emissions (He et al., 2017), and thus it is important to know the effect of the Fe/N ratio on the NRFO process with regards to yield of N_2O, one of the products of chemodenitrification (Eq. 4). Chemodenitrification accounted for 15-25% of the total N_2O production from marine sediments, indicating the importance of N_2O production from chemodenitrification (Otte et al., 2019). In the current study, the occurrence of the highest N_2O accumulation in the high Fe/N ratio treatments was attributed to enhanced chemodenitrification and NO_2^- reduction due to the high Fe(II) concentrations. Although the observed N_2O production was much lower than the N_2 production, it has important implications for the greenhouse effect as the global warming potential of N_2O is 300 times that of CO_2 on a 100-year scale (IPCC, 2013). Hence, NRFO processes may be notable sources of N_2O in Fe-rich habitats. Although enzymatic denitrification can reduce N_2O to N_2 under anoxic conditions (Zhu-Barker et al., 2015), the higher N_2O accumulations in the high Fe/N ratio treatments in the current study indicate that enzymatic denitrification in the transformation of N_2O to N_2 was inhibited (Fig. 8). This could be attributed to a decrease of the metabolic capabilities of these bacteria at high Fe/N ratios, caused by the precipitation and encrustation of Fe (Chakraborty et al., 2011; Liu et al., 2019).

At 132 h, the dominant N denitrification product was N_2, which accounted for ≥56% of the reduced NO_3^- in all Fe/N ratio treatments (Fig. 9). Hence, in oxygen minimum zones an appreciable amount of N_2 emission is a promising way to permanently remove reactive N from Fe-rich habitats.

The highest N_2 production (Fig. 3b) and percentage N_2 of reduced NO_3^- (81.2% at 132 h) occurred at a Fe/N ratio of 6, where the actual ratio between Fe(II) oxidation and the net NO_3^- reduction was 5.37, close to the theoretical value that can be obtained from Eq. 5 (Straub et al., 1996) for NRFO organisms:

$$10\ Fe^{2+} + 2\ NO_3^- + 24\ H_2O \rightarrow 10\ Fe(OH)_3 + N_2 + 18\ H^+ \quad \text{(Eq. 5)}$$

Considering that the formation of N_2O has a negative effect on the atmosphere, while complete denitrification with the formation of N_2 has almost no effect (Włodarczyk et al., 2019), a Fe/N molar ratio of 6 is the optimum for formation of N_2, to ensure the most complete denitrification process.

The observed N_2 production in the treatments with Fe/N ratios of 8-10 were lower than that in other treatments (Fig. 9), and was attributed to that further enzymatic reduction of N_2O to N_2 was likely severely hampered at high Fe/N ratios due to coating of cells with Fe minerals (Fig. 8).

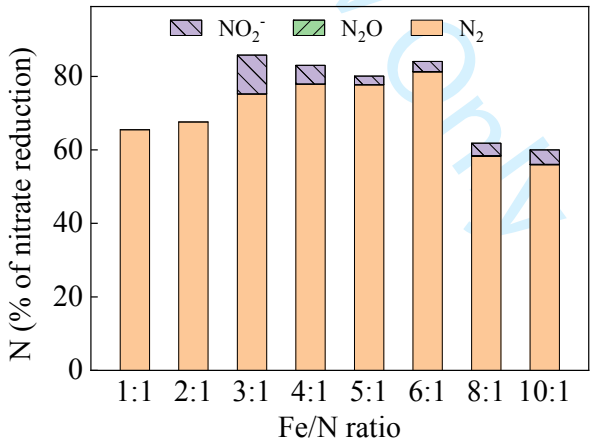

Fig. 9. Percentage contribution of the N products of denitrification (NO_2^-, N_2O and N_2) to NO_3^- reduction from different Fe/N ratio treatments after 132 h incubation.

4.2. Fe transformation

NRFO bacteria have been demonstrated to oxidize both soluble and insoluble Fe(II) (Carlson

et al., 2012). Vivianite with a K_{sp} of 10^{-36} is a very stable Fe(II) mineral (Miot et al., 2009a), although it has been shown to be oxidized (~0.5 mmol Fe(II) over 24 h) by *Acidovorax ebreus*, but only in the presence of an organic cosubstrate (Carlson et al., 2013). The vivianite detected in precipitates in the current study might not be utilized, especially at high Fe/N ratios, as the Fe minerals produced during NRFO has a very low solubility at circumneutral pH (Jamieson et al., 2018). Furthermore, the solubility of Fe(III) increases with decreasing pH values (Weber et al., 2006), probably accounting for the occurrence of the highest concentrations of Fe(III) in solution in the current study in the treatments with the higher Fe/N ratios and also the lower pH (Fig. 4b, Fig. A2). Apart from pH, the concentration of Fe(III) in solution was also affected by the type of Fe(III) minerals; the soluble Fe concentration of ferrihydrite and goethite at pH 7 is $10^{-3.1}$ μmol/L and $10^{-10.9}$ - $10^{-5.9}$ μmol/L, respectively (Schwertmann, 1991). Meanwhile, the oxidation of Fe(II) species during the NRFO process can result in the precipitation of a variety of Fe(III) minerals (Liu et al., 2019). With strong complexing ligands (e.g., CO_3^{2-}) in the system, precipitated Fe tends to form goethite (Bryce et al., 2018). In the current anoxic systems, the formation of goethite was observed at 60 h and 132 h in the treatments with high Fe/N ratios.

The combination of XRD analysis and sequential extraction for Fe fractions is helpful to better understand the type and amount of different Fe minerals produced during the incubation. The pH of the medium solution decreased from an initial value of 7 to 6.14-6.78 across all treatments over 132 h, with the greatest decrease occurring in the high Fe/N ratio treatments (Fig. A3), in accordance with the probable reactions based on stoichiometry (Ottley et al., 1997). In a slightly acidic anoxic environment, the ionization of HCO_3^- (initial concentration = 22 mmol/L) can produce very small

amounts of CO_3^{2-}, which in turn combine with Fe(II) to form $FeCO_3$. Interestingly, the formation of Fe_{carb} including siderite and ankerite (Poulton and Canfield, 2005) seems to occur only in anoxic habits that are rich in Fe, non-sulfidic, and have a high CO_3^{2-} content (Aller et al., 2004). Easily reducible oxides (Fe_{ox1}) include ferrihydrite and lepidocrocite, while reducible oxides (Fe_{ox2}) include goethite, hematite, and akaganéite (Poulton and Canfield, 2005). Taken together, the results of the XRD analysis and sequential extraction indicated that Fe_{ox1} and Fe_{ox2} in the precipitates included ferrihydrite and goethite, respectively. The Fe_{ox1} fraction accounted for 83.1% and 53.1% of the total Fe in precipitates in the Fe/N ratio treatments of 1 and 2, respectively, showing that easily reducible oxides was the main Fe mineral produced during the NRFO process at Fe/N ratios of 1-2. At Fe/N ratios of 3-10, percentages of the total Fe in precipitates were similar for Fe_{ox1} (29.1-37.9%) and Fe_{ox2} (29.3-42.3%), suggesting the dominant Fe minerals were easily reducible oxides and reducible oxides. A marginal amount of Fe_{mag} (0.02%-0.16%) was observed by sequential extraction of Fe precipitates across all treatments, and magnetite was also identified by XRD. The presence of vivianite was detected in the precipitates by XRD analysis, but the sequential extraction procedure used in the current study was not suitable to specifically identify vivianite. Different Fe minerals have different capacities for combining with contaminants such as metal/metalloids and phosphorus, and thus play different roles in aquatic geochemistry. Hence, the interaction between the Fe/N ratio and NRFO processes may influence not only NO_3^- reduction but also the quantity and composition of Fe oxidation products with different environmental behavior. The results may shed light on the denitrification characteristics and Fe transformation process mediated by Fe/N molar ratios in Fe-rich anoxic zones in both natural aquatic environments and

wastewater treatment systems.

5. Conclusions

NO_3^- reduction coupled with Fe(II) oxidation was mediated by *Paracoccus denitrificans* in incubation experiments of 132 h duration, with different initial Fe/N molar ratios. NO_3^- reduction decreased as the Fe/N ratio increased from 1 to 10. Considerable NO_2^- accumulation, equivalent to >30% of the reduced NO_3^-, was observed at Fe/N ratios of 2-5 within 60 h. N_2O emissions increased notably with increasing Fe/N ratios. Maximum production of N_2 occurred at an initial Fe/N molar ratio of 6, higher than at other Fe/N ratios investigated, and accounted for 81.2% of the reduction of NO_3^-. Ferrihydrite, goethite, vivianite and magnetite were identified by XRD in Fe precipitates sampled after 132 h. The dominant Fe minerals were easily reducible oxides at Fe/N ratios of 1-2, and easily reducible oxides and reducible oxides at Fe/N ratios of 3-10.

Acknowledgements

This work was supported by the National Key R & D Program of China (No. 2017YFC0505305) and the Fundamental Research Funds for the Central Universities (No. 2662018JC053).

References

Aller R C, Heilbrun C, Panzeca C, Zhu Z, Baltzer F (2017). Coupling between sedimentary dynamics, early diagenetic processes, and biogeochemical cycling in the Amazon - Guianas mobile mud belt: Coastal French Guiana. Marine Geology, 208(2-4): 331–360

APHA (2012). Standard methods for the examination of water and wastewater, 22nd ed. Washington, DC: American Public Health Association

Bryce C, Blackwell N, Schmidt C, Otte J, Huang Y M, Kleindienst S, Tomaszewski E, Schad M, Warter V, Peng C, Byrne J M, Kappler A (2018). Microbial anaerobic Fe(II) oxidation – Ecology, mechanisms and environmental implications. Environmental Microbiology, 20(10): 3462–3483

Buchwald C, Grabb K, Hansel C M, Wankel S D (2016). Constraining the role of iron in environmental nitrogen transformations: Dual stable isotope systematics of abiotic NO_2^- reduction by Fe(II) and its production of N_2O. Geochimica et Cosmochimica Acta, 186: 1–12

Carlson H K, Clark I C, Melnyk R A, Coates J D (2012). Toward a mechanistic understanding of anaerobic nitrate-dependent iron oxidation: Balancing electron uptake and detoxification. Frontiers in Microbiology, 3: 57. doi: 10.3389/fmicb.2012.00057

Carlson H K, Clark I C, Blazewicz S J, Iavarone A T, Coates, J D (2013). Fe(II) oxidation is an innate capability of nitrate-reducing bacteria that involves abiotic and biotic reactions. Journal of Bacteriology, 195(14): 3260–3268

Chakraborty A, Roden E .E, Schieber J, Picardal F (2011). Enhanced growth of *Acidovorax* sp. strain 2AN during nitrate-dependent Fe(II) oxidation in batch and continuous-flow systems. Applied and Environmental Microbiology, 77(24): 8548–8556

Chen D D, Liu T X, Li X M, Li F B, Luo X B, Wu, Y D, Wang, Y (2018). Biological and chemical processes of microbially mediated nitrate-reducing Fe(II) oxidation by *Pseudogulbenkiania* sp. strain 2002. Chemical Geology, 476: 59–69

Chen D D, Yuan X, Zhao W Q, Luo X B, Li F B, Liu T X (2020). Chemodenitrification by Fe(II) and nitrite: pH effect, mineralization and kinetic modeling. Chemical Geology, 541, 119586.

doi: 10.1016/j.chemgeo.2020.119586

Das S, Hendry M J, Essilfie-Dughan J (2011). Transformation of two-line ferrihydrite to goethite and hematite as a function of pH and temperature. Environmental Science & Technology, 45(1): 268–275

Ehrenreich A, Widdle F (1994). Anaerobic oxidation of ferrous iron by purple bacteria, a new type of phototrophic metabolism. Applied and Environmental Microbiology, 60(12): 4517–4526

Grabb K C, Buchwald C, Hansel C M, Wankel S D (2017). A dual nitrite isotopic investigation of chemodenitrification by mineral-associated Fe(II) and its production of nitrous oxide. Geochimica et Cosmochimica Acta, 196: 388–402

Han Z F, Miao Y, Dong J, Shen Z Q, Zhou Y X, Liu S, Yang C P (2019). Enhanced nitrogen removal and microbial analysis in partially saturated constructed wetland for treating anaerobically digested swine wastewater. Frontiers of Environmental Science & Engineering, 13(4): 52. doi: 10.1007/s11783-019-1133-4

He Q, Zhu Y Y, Li G, Fan L L, Ai H N, Huangfu X L, Li H (2017). Impact of dissolved oxygen on the production of nitrous oxide in biological aerated filters. Frontiers of Environmental Science & Engineering, 11(6): 16. doi: 10.1007/s11783-017-0964-0

IPCC (2013). Summary for policymakers. In: Stocker T F, Qin D, Plattner G-K, Tignor M M B, Allen S K, Boschung J, et al. eds. Climate change 2013: The Physical Science Basis. Working Group I Contribution to the Fifth Assessment Report of the Intergovernmental Panel on Climate Change. New York: Cambridge University Press, 3–32

Jamieson J, Prommer H, Kaksonen A H, Sun J, Siade A J, Yusov A, Bostick B (2018). Identifying

and quantifying the intermediate processes during nitrate-dependent iron(II) oxidation. Environmental Science & Technology, 52(10): 5771–5781

Klueglein N, Kappler A (2013). Abiotic oxidation of Fe(II) by reactive nitrogen species in cultures of the nitrate-reducing Fe(II) oxidizer *Acidovorax* sp. BoFeN1 - questioning the existence of enzymatic Fe(II) oxidation. Geobiology, 11(2): 180–190

Liu T X, Chen D D, Luo X B, Li X M, Li F B (2019). Microbially mediated nitrate-reducing Fe(II) oxidation: Quantification of chemodenitrification and biological reactions. Geochimica et Cosmochimica Acta, 256: 97–115

Ma H, Zhao B Y, Li L, Xie F, Zhou H J, Zheng Q, Wang X H, He J, Lu C W (2019). Fractionation trends of phosphorus associating with iron fractions: An explanation by the simultaneous extraction procedure. Soil & Tillage Research, 190: 41–49

Melton E D, Swanner E D, Behrens S, Schmidt C, Kappler A (2014). The interplay of microbially mediated and abiotic reactions in the biogeochemical Fe cycle. Nature Reviews Microbiology, 12(12): 797–808

Miot J, Benzerara K, Morin G, Bernard S, Beyssac O, Larquet E, Kappler A, Guyot F (2009a). Transformation of vivianite by anaerobic nitrate-reducing iron-oxidizing bacteria. Geobiology, 7(3): 373–384

Miot J, Benzerara K, Morin G, Kappler A, Bernard S, Obst M, Férard C, Skouri-Panet F, Guigner J M, Posth N, Galvez M, Brown G E, Guyot F (2009b). Iron biomineralization by anaerobic neutrophilic iron-oxidizing bacteria. Geochimica et Cosmochimica Acta, 73(3): 696–711

Miot J, Remusat L, Duprat E, Gonzalez A, Pont S, Poinsot M (2015). Fe biomineralization mirrors

individual metabolic activity in a nitrate-dependent Fe(II)-oxidizer. Frontiers in Microbiology, 6: 879. doi: 10.3389/fmicb.2015.00879

Muehe E M, Gerhardt S, Schink B, Kappler A (2009). Ecophysiology and the energetic benefit of mixotrophic Fe(II) oxidation by various strains of nitrate-reducing bacteria. FEMS Microbiology Ecology, 70(3): 335–343

Otte J M, Blackwell N, Ruser R, Kappler A, Kleindienst S, Schmidt C (2019). N_2O formation by nitrite-induced (chemo)denitrification in coastal marine sediment. Scientific Reports, 9: 10691. doi: 10.1038/s41598-019-47172-x

Ottley C J, Davison W, Edmunds W M (1997). Chemical catalysis of nitrate reduction by iron(II). Geochimica et Cosmochimica Acta, 61(9): 1819–1828

Picardal F (2012). Abiotic and microbial interactions during anaerobic transformations of Fe(II) and NO_x^-. Frontiers in Microbiology, 3: 112. doi: 10.3389/fmicb.2012.00112

Posth N R, Canfield D E, Kappler A (2014). Biogenic Fe(III) minerals: From formation to diagenesis and preservation in the rock record. Earth-Science Reviews, 135: 103–121

Poulton S W, Canfield D E (2005). Development of a sequential extraction procedure for iron: Implications for iron partitioning in continentally derived particulates. Chemical Geology, 214(3-4): 209–221

Pownceby M I, Hapugoda S, Manuel J, Webster N A S, MacRae C M (2019). Characterisation of phosphorus and other impurities in goethite-rich iron ores – Possible P incorporation mechanisms. Minerals Engineering, 143: 106022. doi: 10.1016/j.mineng.2019.106022

Schwertmann U (1991). Solubility and dissolution of iron oxides. Plant and Soil, 130(1-2): 1–25

Sears, H J, Spiro S, Richardson D J (1997). Effect of carbon substrate and aeration on nitrate reduction and expression of the periplasmic and membrane-bound nitrate reductases in carbon-limited continuous cultures of *Paracoccus denitrificans* Pd1222. Microbiology, 143(12): 3767–3774

Sparacino-Watkins C, Stolz J F, Basu P (2014). Nitrate and periplasmic nitrate reductases. Chemical Society Reviews, 43(2): 676–706

Stookey L L (1970). Ferrozine - a new spectrophotometric reagent for iron. Analytical Chemistry, 42(7): 779–781

Straub K L, Benz M, Schink B, Widdel F (1996). Anaerobic, nitrate-dependent microbial oxidation of ferrous iron. Applied and Environmental Microbiology, 62(4): 1458–1460

Vasilaki V, Volcke E I P, Nandi A K, van Loosdrecht M C M, Katsou E (2018). Relating N_2O emissions during biological nitrogen removal with operating conditions using multivariate statistical techniques. Water Research, 140: 387–402

Wang M L, Hu R G, Zhao J S, Kuzyakov Y, Liu S R (2016). Iron oxidation affects nitrous oxide emissions via donating electrons to denitrification in paddy soils. Geoderma, 271: 173–180

Watsuntorn W, Ruangchainikom C, Rene E R, Lens, P N L, Chulalaksananukul W (2019). Comparison of sulphide and nitrate removal from synthetic wastewater by pure and mixed cultures of nitrate-reducing, sulphide-oxidizing bacteria. Bioresource Technology, 272: 40–47

Weber K A, Achenbach L A, Coates J D (2006). Microorganisms pumping iron: Anaerobic microbial iron oxidation and reduction. Nature Reviews Microbiology, 4(10): 752–764

Włodarczyk T, Balakhnina T, Matichenkov V, Brzezińska M, Nosalewicz M, Szarlip P, Fomina I

(2019). Effect of silicon on barley growth and N_2O emission under flooding. Science of the Total Environment, 685: 1–9

Zhang L H, Zheng J, Guo J B, Guan X H, Zhu S Y, Jia Y P, Zhang J, Zhang X Y, Zhang H F (2019). Effects of Al^{3+} on pollutant removal and extracellular polymeric substances (EPS) under anaerobic, anoxic and oxic conditions. Frontiers of Environmental Science & Engineering, 13(6): 85. doi: 10.1007/s11783-019-1169-5

Zhang M, Zheng P, Li W, Wang R, Ding S, Abbas G (2015). Performance of nitrate-dependent anaerobic ferrous oxidizing (NAFO) process: A novel prospective technology for autotrophic denitrification. Bioresource Technology, 179: 543–548

Zhang M, Zheng P, Wang R, Li W, Lu H.F, Zhang J Q (2014). Nitrate-dependent anaerobic ferrous oxidation (NAFO) by denitrifying bacteria: A perspective autotrophic nitrogen pollution control technology. Chemosphere, 117: 604–609

Zhao L D, Dong H L, Kukkadapu R, Agrawal A, Liu D, Zhang J, Edelmann R E (2013). Biological oxidation of Fe(II) in reduced nontronite coupled with nitrate reduction by *Pseudogulbenkiania* sp. Strain 2002. Geochimica et Cosmochimica Acta, 119: 231–247

Zhu-Barker X, Cavazos A R, Ostrom N E, Horwath W R, Glass J B (2015). The importance of abiotic reactions for nitrous oxide production. Biogeochemistry, 126: 251–267

Zorgani E A, Cibati A, Trois C (2016). Assessment of a natural iron-based sand for the removal of nitrate from water. Water Air & Soil Pollution, 227, 249. doi: 10.1007/s11270-016-2942-8

Appendix A:

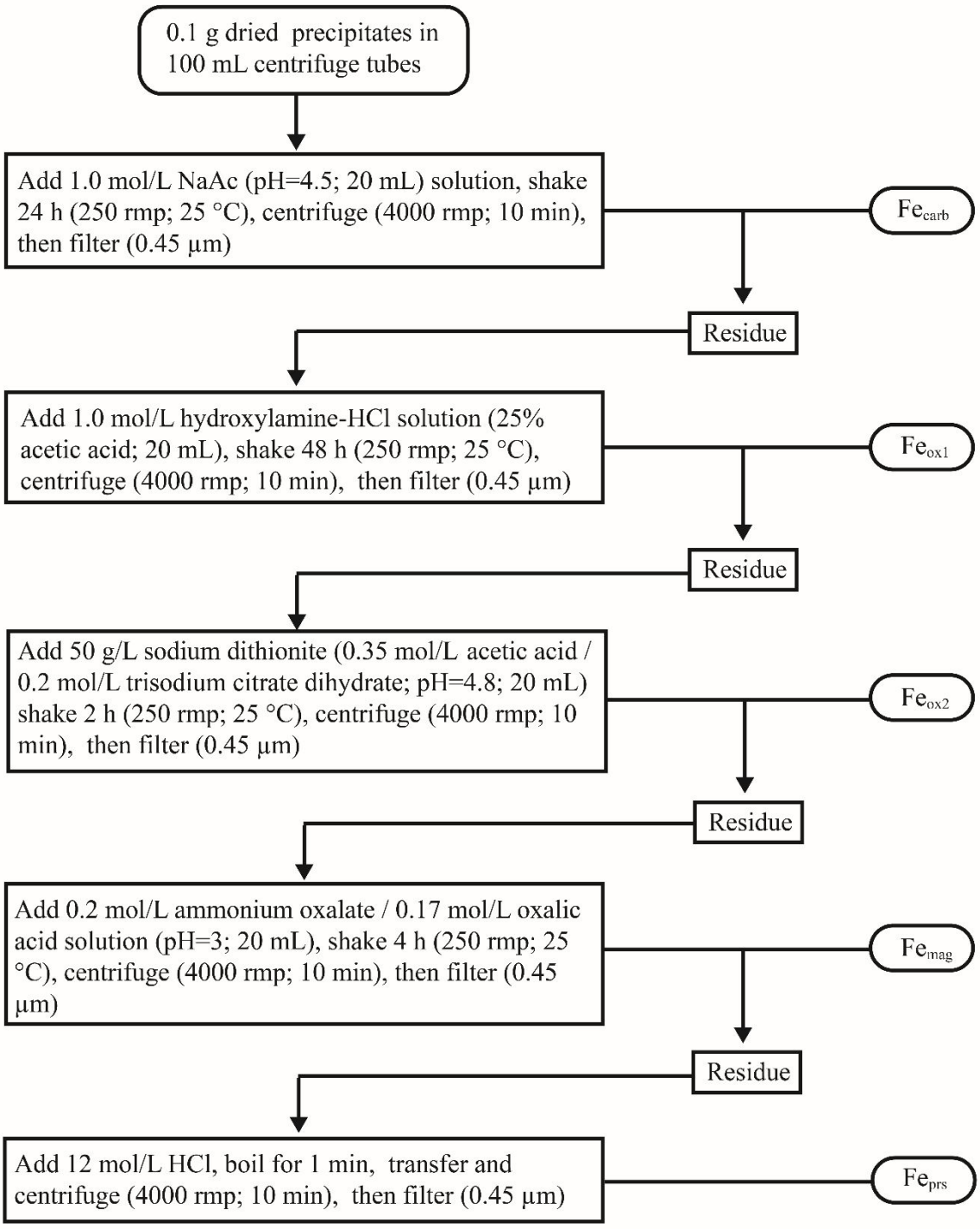

Fig. A1 Sequential extraction procedure for Fe in precipitates (Ma et al., 2019).

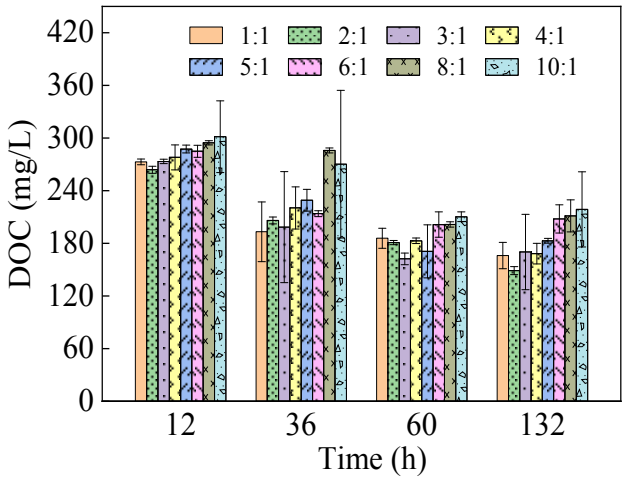

Fig. A2 Dissolved organic carbon (DOC) concentrations at different Fe/N ratios during the incubation.

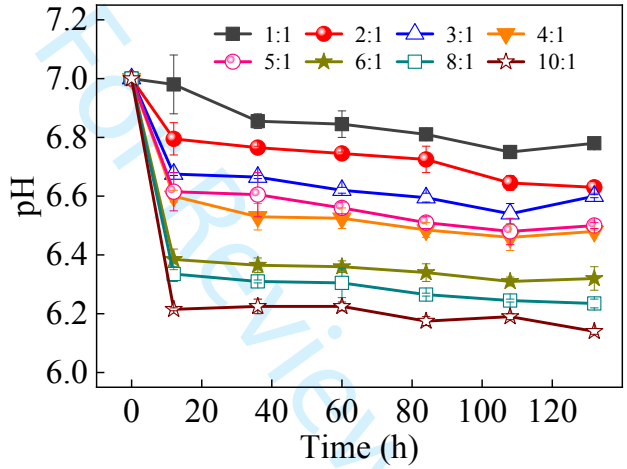

Fig. A3 Solution pH at different Fe/N ratios during the incubation.

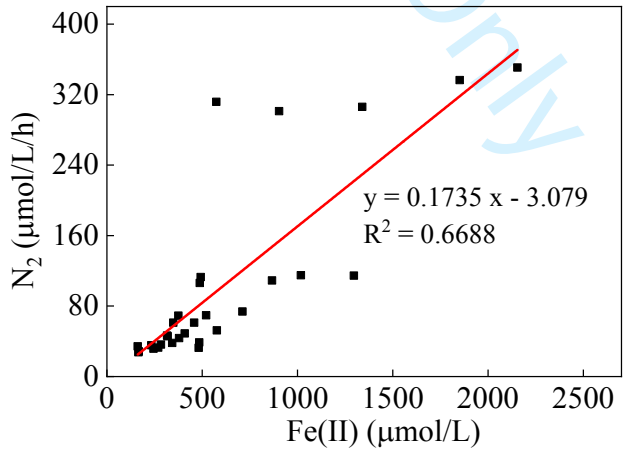

Fig. A4 Relationship between Fe(II) concentrations in the medium and N_2 fluxes in treatments with Fe/N ratios of 1-5 during the incubation.

Table A1 Change in nitrate concentrations (ΔNO_3^-), Fe^{2+} concentrations (ΔFe^{2+}) and DOC concentrations (ΔDOC) under different initial Fe/N ratios after 132 h. Different letters in the same column indicate significant differences (P<0.05, n=3).

Fe/N ratio	ΔNO_3^- (mmol/L)	ΔFe^{2+} (mmol/L)	ΔDOC (mg/L)
1:1	0.938 ± 0.006 bc	0.835 ± 0.012 f	144 ± 15.0 ab
2:1	0.934 ± 0.004 c	1.83 ± 0.010 e	161 ± 4.60 a
3:1	0.948 ± 0.004 a	2.76 ± 0.005 d	140 ± 42.9 ab
4:1	0.934 ± 0.003 c	3.73 ± 0.008 c	142 ± 11.7 ab
5:1	0.944 ± 0.002 ab	4.52 ± 0.042 b	127 ± 2.80 ab
6:1	0.940 ± 0.005 abc	4.90 ± 0.205 b	102 ± 16.1 b
8:1	0.907 ± 0.008 d	5.94 ± 0.437 a	98.9 ± 18.3 b
10:1	0.886 ± 0.002 d	6.10 ± 0.488 a	91.6 ± 42.8 b

Table A2 Concentrations of different Fe forms in the precipitates obtained from different Fe/N ratios.

Fe fraction	Fe concentrations (mg/g)							
	Fe/N 1	Fe/N 2	Fe/N 3	Fe/N 4	Fe/N 5	Fe/N 6	Fe/N 8	Fe/N 10
Fe_T	196	248	292	296	286	326	328	336
Fe_{carb}	1.85	7.08	3.27	4.32	2.93	7.83	10.3	11.9
Fe_{ox1}	163	132	92.9	86.1	108	117	124	122
Fe_{ox2}	17.0	90.1	116	125	112	124	122	98.4
Fe_{mag}	0.070	0.390	0.220	0.130	0.060	0.130	0.070	0.120
Fe_{prs}	0.960	1.45	0.310	0.100	0.520	0.500	0.260	0.200
Fe_U	13.3	17.4	78.6	80.1	61.9	76.9	70.4	103

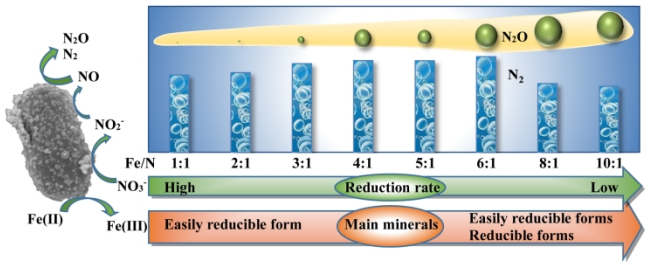

209x297mm (300 x 300 DPI)